DOI: 10.1002/ ((please add manuscript number))
Article type: Full paper

Highly Sensitive Metabolite Biosensor based on Organic Electrochemical Transistor Integrated with Microfluidic Channel and Poly(N-vinyl-2-pyrrolidone)-Capped Platinum Nanoparticles

By *Xudong Ji, Ho Yuen Lau, Xiaochen Ren, Boyu Peng, Peng Zhai, Shien-Ping Feng and Paddy K. L. Chan**

Xudong Ji, Ho Yuen Lau, Xiaochen Ren, Boyu Peng, Peng Zhai, Prof. Shien-Ping Feng, Prof. Paddy K. L. Chan
Department of Mechanical Engineering
The University of Hong Kong
Pokfulam Road
Hong Kong
E-mail: pklc@hku.hk

Key words: Organic electrochemical transistor, bioelectronics, enzymatic biosensor

Abstract

Organic electrochemical transistors (OECTs) are used as highly sensitive glucose and lactate sensors by modifying the gate electrode with glucose oxidase/lactate oxidase and poly(n-vinyl-2-pyrrolidone)-capped platinum nanoparticles (Pt NPs). The Pt NPs are deposited by using a two-step dip coating method without bias instead of the conventional electro-deposition method and followed by a UV-Ozone post treatment to enhance the catalytic ability of the Pt NPs. The modified OECT sensors have extremely high sensitivity, and can achieve a detection limit of glucose and lactate down to 10^{-7} M and 10^{-6} M respectively. A polydimethylsiloxane microfluidic channel is successfully integrated with the OECT sensors, which provides a compact chip size of the sensors, a short detection time of around one minute and extremely low consumption of analyte (30 μL). The cross talk between individual sensors in multi-analyte sensing devices is reduced by the dual microfluidic channel structure. Practical applications, such as for detecting glucose in saliva, can therefore be realized, and a prototype of a portable

glucose sensor has been successfully created in this study. This portable glucose sensor has excellent potential for real-time and non-invasive glucose sensing applications.

1. Introduction

Organic electrochemical transistors (OECTs) have been successfully applied in organic bioelectronics recently, and can detect biological analyte concentrations, [1-5] interface with the human brain, [6-8] monitor cell activities [9-11] as well as sense electrocardiography (ECG) signals. [12,13] Among all of these applications, OECTs applied as glucose sensors have attracted particular attention due to their high sensitivity, and in particular, are suitable for non-invasive detection of glucose in saliva with extremely low glucose concentrations that range from 0.008 to 0.21 mM [14]. This non-invasive method has excellent potential in replacing traditional blood glucose testing methods which are invasive and run the risk of infection. Zhu *et al*. and Macaya *et al*. first demonstrated the use of OECTs for glucose sensing [15,16], where an electrolyte was blended with glucose oxidase (GOx) in a polydimethylsiloxane (PDMS) reservoir with a single platinum (Pt) wire electrode, with a detection limit down to several μM. However, the floating structure required the re-deposition of the GOx enzyme each time after use and a single Pt wire gate without any modifications also limited the sensitivity. Tang *et al.* developed an OECT based glucose sensor where the gate electrode was modified by using multi-walled carbon nanotubes/platinum nanoparticles (Pt NPs) and GOx. [17] The detection limit was significantly improved to 5 nM due to the high catalytic ability of the Pt NPs. However, the large electrolyte containers used in the device cause large analyte consumption and a longer detection time, and are unsuitable for portable applications. As a result, it will be very useful if a highly sensitive glucose sensor with a quick response that only requires a small amount of analyte and minimum operating power can be developed.

Actually, glucose can also be transferred into lactate through anaerobic respiration during intensive exercise, [18] and thus instead of sensing the glucose concentration, one can also sense

the lactate concentration in the body fluids to evaluate the level of the intensity of exercise. Furthermore, this coupled relationship provides a more accurate way to determine the sensed glucose concentrations in human body fluids like saliva. Therefore, a bio-sensor with multi-analyte sensing capability is important for precise healthcare monitoring on a daily basis. In conventional OECT-based enzymatic sensors, Pt NPs are generally used on the gate electrode and deposited by electro-deposition due to the high catalytic ability of Pt and the extremely large surface area of NPs. Since this deposition method requires additional voltage bias from a three terminal potentiostat, [17, 19] the cost of the fabrication, time and complexity will be increased. Therefore, if a simple but efficient way to deposit Pt NPs onto these devices is available, that would be an important cornerstone for the development of OECT sensors.

In this study, we have deposited Pt NPs onto the gate electrode of an OECT sensor by using a two-step dip coating method without bias. We report a highly sensitive glucose and lactate sensor with a detection limit of 10^{-7} M and 10^{-6} M respectively by integrating the OECT with a microfluidic channel. The total volume of the microfluidic channel is only around 3 mm^3, which is suitable for low-doses, allows fast detection and is compatible with lab-on-a-chip applications. Multi-sensing is carried out by a dual microfluidic channel to simultaneously detect both glucose and lactate. We have also proceeded a step further to utilize 3D printing for the development of a prototype of a portable glucose sensor which can be integrated with a smartphone via Bluetooth connection. The highly comparable results between the portable sensor and the device under laboratory settings indicate the excellent potential of applying the glucose sensor in real-time non-invasive monitoring of glucose.

2. Results and Discussion

2.1 Electrical Properties and Sensing Mechanism of OECT-based Glucose Sensor

Figure 1a, b schematically shows the OECT-based glucose sensor and the modification of the gate electrode respectively. The fabrication details of the device are discussed in the

experimental section. The PDMS channel has a rectangular cross-section with a height of 50 μm and width of 4.5 mm. The PDMS channel is directly attached on top of the active layer of the OECT. Phosphate buffered saline (PBS; 3 μL) electrolyte was injected into the PDMS channel to act as the ion exchange medium. Typical transfer and output curves of the device are shown in Figure 1c, d. One of the major advantages of using OECTs as a sensor is their high transconductance (up to an mS range compared to conventional OFETs) defined by $g_m = \Delta I_D / \Delta V_G$ [20]. The high transconductance of OECTs with a polarizable gate such as gold and platinum can be achieved by a large area ratio between the gate electrode (A_g) and active channel (A_{ch}) (large A_g/A_{ch} value). [21, 22] For our device, the A_g/A_{ch} ratio is 45 and the maximum transconductance is 1.5 mS. The comparable transconductance value of our device with other OECT devices that have a large beaker reservoir [3, 20] allows high sensitivity even extremely low volume of electrolyte is required in our device.

In the OECT structure, enzymes immobilized on the gate electrode catalyze the analyte (glucose in our case) to produce hydrogen peroxide (H_2O_2). The electrochemical oxidation of H_2O_2 is catalyzed by the gate electrode when a positive bias is applied. The oxidation process results in the transfer of electrons to the gate electrode and changes the electrical double layer at the gate/electrolyte interface, which reduces the voltage drop at the gate/electrolyte interface and hence increases the potential that is applied to the active channel. The corresponding effective gate voltage V_G^{eff} of the transistor is given by: [23]

$$V_G^{eff} = V_G + (1+\gamma)\frac{\kappa T}{2q}\ln[H_2O_2] + \text{constant} \quad (1)$$

where γ is the ratio between the capacitance of the two interfaces: electrolyte/channel interface (C_c) and electrolyte/gate interface (C_G), $\gamma = C_c/C_G$, κ is the Boltzmann constant,

and *T* is the temperature. Therefore, an increase in the concentration of H_2O_2 would increase the effective gate voltage and hence decrease the channel current of the device. By monitoring the channel current and changes in the effective gate voltage, we can measure the glucose concentration in the analyte.

2.2 Characterization of Pt NPs Modified Electrodes with Different Post Treatment Methods

Pt NPs are a key element for catalyzing the oxidation of H_2O_2, thus improving the sensitivity of OECT-based glucose sensors. [17] Instead of using conventional electro-deposition, we applied a two-step dip coating method without bias for the deposition of the Pt NPs. [24] We first used a surface conditioner which is commonly used on printed circuit boards (PCBs) as a grafting agent to change the surface charge state on the gold (Au) electrode before coating the poly(N-vinyl-2-pyrrolidone) (PVP)-capped Pt NPs. This step can significantly enhance the electrostatic force between the NPs and the electrode, which allows for the better absorption of the NPs on the electrode. After the deposition of the NPs, they were treated by using two different methods, (i) UV-Ozone and (ii) thermal annealing, to separately remove the PVP capping layer and thus enhance the catalytic ability of the Pt NPs. **Figure 2**a shows the electrochemical performance of the Au/Pt NPs electrode after the UV-Ozone post treatment (Line I) and Au/Pt NPs electrode after thermal annealing post treatment (Line II). Line I shows a higher peak current density, thus indicating that the Au/Pt NPs electrode has a larger active surface area after the UV-Ozone post treatment as opposed to the Au/Pt NP electrode that underwent thermal annealing post treatment. Figure 2b shows the surface capacitances of these two electrodes and a bare Au electrode characterized in a PBS solution at zero bias voltage. The capacitances at low frequencies are regarded as approximately proportional to the surface areas of the electrodes. It can be observed that the surface area of the Au/Pt NPs electrode after the UV-Ozone post treatment is around 5 times greater than that of the bare Au electrode and 2.5

times than Au/Pt NPs electrode after thermal annealing post treatment. Figure 2c shows the atomic force microscopy (AFM) image of Au/Pt NPs electrode after the UV-Ozone post treatment. The RMS roughness is 3.6 nm. However, the RMS roughness of the Au/Pt NPs electrode after thermal annealing post treatment is around 5.1 nm as shown in Figure 2d. The higher surface roughness of the Au/Pt NPs electrode after thermal annealing post treatment is attributed to the aggregation of the Pt NPs. Such effect has been verified by transmission electron microscopy (TEM) of the PVP-capped Pt NPs coated gate electrodes before and after thermal annealing or UV-Ozone post treatment as shown in **Figure S1**. It can be clearly seen that the diameter of Pt NPs underwent thermal annealing post treatment is significantly larger than that after UV-Ozone post treatment. One possible reason for the Pt NPs aggregation in thermal annealing post treatment is due to the cross-linking of PVP as previously reported. [25, 26] The performance of the devices underwent these two post treatment methods will be discussed later to verify the influence of Pt NPs aggregation on the sensitivity of the devices.

2.3 OECT for Sensing Glucose and Lactate

The OECT devices were first calibrated by injecting different concentrations of a glucose solution into the microfluidic channel at a flow rate 2 μL s^{-1} with a total injection volume of 30 μL. To compare the response of the drain source current after the injection of the glucose, the normalized current (*NC*) was calculated in accordance with the following equation:

$$NC = \left| \frac{I_D^{Conc=c}}{I_D^{Conc=0}} \right| \quad (2)$$

where $I_D^{Conc=0}$ and $I_D^{Conc=c}$ are the channel current before and after the injection of the glucose with the concentration of interest, respectively. As expected, the *NC* decreases after the injection of the glucose solution. As for the device that underwent the UV-Ozone post treatment,

the reduced *NC* after glucose injection is shown in **Figure 3**a. It can be clearly observed from the magnified plot in Figure 3b that the glucose detection limit is 10^{-7} M. The detection time of the microfluidic channel device is around 1 min, which is much faster than conventional OECT-based glucose sensors with a large reservoir. [17, 29] For the device that underwent thermal annealing post treatment, the detection limit is one magnitude lower than the device that underwent the UV-Ozone post treatment, or 10^{-6} M (Figure 3c). By comparing the effective gate voltage shift ΔV_G^{eff} caused by the glucose solution of these two devices (Figure 3d), we could clearly see that the device that underwent the UV-Ozone post treatment has a better performance compared with the device that underwent thermal annealing post treatment. Since the catalytic ability of the gate electrode will determine the sensing ability of the device, and the catalytic ability is intrinsically determined by the active surface area of the Pt NPs. The improvement in the detection limit of the device that underwent the UV-Ozone post treatment could be attributed to the higher active surface area of the Pt NPs on the gate electrode.

Similarly, the sample that underwent UV-Ozone post treatment can also be used as a lactate sensor by changing the enzyme from GOx to lactate oxidase (LOx). As shown in **Figure 4**, the detection limit of lactate is 10^{-6} M, which is lower than that of the glucose sensor device fabricated under the same conditions. This is attributed to the lower concentration of LOx enzymes that was used (0.625 mg mL^{-1}, 113 U mg^{-1}) in comparison to the concentration of GOx enzymes (15 mg mL^{-1}, 15 U mg^{-1}) in the glucose sensor. Although the detection limit of the lactate sensor is not as high as that of the glucose sensor, it is sufficient to address the range of lactate concentration found in human body fluids, such as sweat. [27]

2.4 OECT-based Multi-Analyte Sensor

The high-performance glucose and lactate sensors allowed the implementation of a more complicated analysis which is the simultaneous detection of glucose and lactate levels in one

analyte. The glucose and lactate sensors are combined together into one microfluidic chip with a dual channel as shown in **Figure 5**a. An analyte with a different composition was injected into the dual microfluidic channel for characterization purposes. A pure PBS solution was used as the reference sample (see Figure 5b), which showed almost no influence on the current in both the glucose and lactate sensors. After that, we increased the concentration of the glucose and lactate in the analyte solution respectively. As shown in Figure 5c, 10^{-5} M of lactate causes an obvious decrease in the channel current in the lactate sensor, while the current in the glucose sensor remains almost the same. With reference to Figure 5d, further increases of the lactate concentration to 10^{-4} M result in an even higher current change in the lactate sensor, while the current in the glucose sensor remains constant. This suggests that the H_2O_2 in the micro chamber of the lactate sensor did not diffuse to the glucose sensor and thus there is no cross talk between the two sensors. Similar, as shown in Figures 5e, f, an increased glucose concentration clearly causes changes in the current in the glucose sensor while there are nearly no changes in the lactate sensor. After confirming that there are no unwanted signal transfers between the two devices, a mixed solution of glucose and lactate was characterized by the combined sensor. As shown in Figure 5g~i, the different glucose and lactate concentrations can be clearly differentiated, which clearly demonstrates that our device has the potential for the multiple sensing of analyte that has complicated components.

2.5 OECT-based Glucose Sensor for Sensing Salivary Glucose

After we proved that the OECT-based glucose and lactate sensor is highly sensitive, we applied the sensor to non-invasively detect glucose in human saliva. Saliva samples from healthy individuals (P_1, P_2) and diabetic patients (P_3, P_4) collected two hours after lunch were diluted 10 times by using a PBS solution for characterization purposes. Human saliva is a complicated fluid that has several electro-active compounds such as uric acid (UA) and ascorbic acid (AA), which may cause interference in determining glucose. [28] In order to eliminate these

interferences, we added a negatively charged nafion layer before coating the chitosan/GOx layer (**Figure 6**a). The diffusion of the anionic substances, AA and UA, were largely suppressed by using electrostatic interaction. [29] The calibration curve of the device performance over a pure glucose solution is shown in Figure 6b. A reference sensor with a gate that has not been modified by GOx was used to characterize the reduction in the channel current caused by interference other than glucose in the saliva. As shown in **Figure S2**, the difference between the decrease in the *NC* of the glucose and reference sensors is considered to be the real glucose level in the human saliva samples. After calculating the ΔV_G^{eff} caused by four different saliva samples (Figure 6c), it was found that the saliva samples from the diabetic patients cause an obviously larger change in the ΔV_G^{eff} as opposed to the healthy individuals. By transferring the ΔV_G^{eff} to the glucose concentration, the glucose concentration in the saliva of two of the diabetic patients, namely P_3 and P_4, was found to be 0.146 ± 0.014 mM and 0.22 ± 0.019 mM respectively, which are much higher than that of the healthy individuals, namely, P_1 and P_2, whose salivary glucose concentration is 0.074 ± 0.003 mM and 0.0485 ± 0.001 mM respectively. Another practical application for comparing the salivary glucose concentration in the healthy individuals before and after their meal was also carried out by using the same strategy. As shown in **Figure S3**, the glucose level in the human saliva samples increases from 4.2×10^{-5} M to 1×10^{-4} M, which agrees well with the normal salivary glucose concentration of a healthy person. [30]

2.6 Portable Glucose Sensor by Integrating OECT with Smartphone via Bluetooth

Based on the success of the microfluidic channel device, a prototype of a portable glucose sensor to be used for real time diagnosis was made by linking a smartphone with an OECT-based glucose sensor through Bluetooth connection (as shown in **Figure 7**a)**.** In the portable glucose sensor, a resistor was added to the drain source circuit (Figure 7c) so as to convert

current signals into voltage signals. The transfer curve of the device after adding a resistor in the drain source circuit (Figure 7d) showed that the drain source current is substantially reduced due to the additional resistor, which decreased the relative resistance change in the entire circuit. A data acquisition dock was used to provide two constant voltages to drive the device and measure the voltage changes induced by the glucose. The voltage change was sent out to a smartphone via Bluetooth connection and displayed in the interface of the related app (Figure 7b). The data acquisition dock is composed of three major components: Bluetooth low energy (BLE) embedded microcontroller unit (MCU), higher precision analog-digital-converter (ADC) and digital-analog converter (DAC). The MCU (Atmega 328) is a small electronic device that is able to receive, process and output electronic signals. The BLE unit (Texas Instrument CC2540) is embedded in the MCU circuit to provide wireless communication. BLE is a wireless technology that works with various wireless applications to allow reduced power consumption and lower cost compared to conventional Bluetooth. Extra ADC (Texas Instrument ADS1220) and DAC (Microchip MCP4725) modules were added into the MCU to improve the range of measurement and the supplied gate voltage. The whole system was then optimized through programming by using C language which can measure voltage down to 10^{-3} V and provide a stable voltage down to 10^{-1} V. By sliding the tab bar on top of the app interface, a real time graph of the data is shown. Meanwhile, all data, including date, time and measured voltage, were stored in the internal storage of the smartphone for future analysis. To verify the accuracy of our portable glucose sensor, the smartphone-based measurements were compared with those based on a laboratory source meter, see Figure 7e. Glucose solutions of five different concentrations were tested and verified the accuracy of our portable glucose sensor.

3. Conclusion

In summary, we have demonstrated a highly sensitive OECT sensor for glucose and lactate sensing with a detection limit down to 10^{-7} M and 10^{-6} M by using a Pt NPs deposition method

without bias. A microfluidic channel is directly applied on top of the OECT device to reduce the volume of analyte and increase the detection speed. A two-step dip coating method without bias is used to deposit the Pt NPs so as to enhance the device performance. Multiple sensing is demonstrated to be possible by integrating two single devices with two separate channels in one chip. Based on the high sensitivity of the resultant device, we have also successfully performed noninvasive testing of human saliva among normal individuals and diabetic patients, as well as tested the glucose levels in their saliva before and after a meal. Finally, a prototype of a portable glucose sensor for the real time sensing of glucose is created by linking a smartphone with our device through Bluetooth connection. It is anticipated that such a highly sensitive, multi-functional and portable bio-sensor will be a promising means of home healthcare monitoring.

4. Experimental Section

Materials: LOx (113 U mg^{-1}) was purchased from Sorachim. Poly(3,4-ethylenedioxythiophene)-poly(styrenesulfonate) (PEDOT:PSS, PH 1000) was purchased from Clevios. PVP (M.W.8000) was purchased from Acros Organics, and the conditioner (ML-371) from Rockwood Electrochemicals Asia Ltd. All of the other chemicals were purchased from Sigma-Aldrich and used as received.

Synthesis of PVP-capped Pt NPs: The PVP-capped Pt NPs were synthesized in accordance with a protocol developed by Wei et al. [31] First, 1 g of a chloroplatinic acid hexahydrate ($H_2PtCl_6 \cdot 6H_2O$, ≥37.50% Pt basis) precursor was dissolved in 200 mL of deionized (DI) water under stirring. Next, 500 mg of PVP with a molecular weight of 8000 was dissolved into this solution. Finally, a reductant sodium borohydride solution (0.125 M) was gradually added until the color of the entire solution changed from brown to black, which indicated the formation of PVP-capped Pt NPs.

Device fabrication: The schematic structure of the device is shown in Figure 1a. The gold drain (100-nm in thickness), source and gate electrodes were deposited onto a pre-cleaned glass substrate by thermal evaporation through a shadow mask. Before the gold deposition, a thin layer of chromium (Cr) with a thickness of approximately 10 nm was deposited to improve the adhesion between the Au electrode and substrate. PEDOT:PSS (2 mL) was mixed with 100 μL of ethylene glycol, 5 μL of dodecyl benzene sulfuric acid (DBSA) and 1 wt% (3-glycidyloxypropyl) trimethoxysilane (GOPS). [32] After that, the mixed PEDOT:PSS solution was spin-coated as the active channel at 2500 rpm for 1 min and followed by thermal annealing at 140 ˚C under a nitrogen (N_2) atmosphere for 1 hour. The gate modification included Pt NPs deposition and enzyme immobilization. A 2-step dip coating method without bias was used to deposit the Pt NPs to enhance the catalytic ability of the gate electrode. The substrate was immersed into 1% conditioner for 5 min at a temperature of 60 ºC followed by immersion into a PVP-capped Pt NPs solution for 5 min at 40 ºC. Before each step, the substrate was rinsed by DI water to remove any residue. Then, the substrate received a UV-Ozone post treatment for 15 min. This process was used to remove the conditioner on the gate electrode underneath the Pt NPs to enhance the contact between the Pt NPs and gate electrode. Another post treatment with thermal annealing (270 ºC, 10 min) was also conducted in another device for comparison purposes. For enzyme immobilization, a GOx (15 U mg^{-1}) stock solution was prepared by dissolving 30 mg of GOx in 2 mL of a PBS solution. A chitosan (CHIT) solution was prepared by dissolving CHIT (50 mg) in an acetic acid solution (10 mL, 50 mM) followed by electromagnetic stirring for one hour. After that, 1 mL of the GOx solution was mixed with 1 mL of the CHIT solution followed by sonication for 20 min before use. The GOx-CHIT mixture solution (10 μL) was drop casted onto the Pt NPs/Au gate and dried at 4 ºC overnight. Finally, the device was rinsed in DI water to remove any non-immobilized enzymes. All of the procedures are the same in the preparation of the lactate sensor, except that a LOx solution

(0.625 mg mL^{-1}) was used instead of a GOx solution. A nafion solution (5% wt) was diluted to 1% wt by using isopropanol and drop casted (5 μL) onto the Pt NPs/Au gate before enzyme immobilization for sensing glucose in saliva. The nafion film form required approximately 30 min in room temperature. The microfluidic channel was fabricated by using conventional photolithography technology and the bonding process between the PDMS-based microfluidic channel with the OECT device was carried out with an oxygen-plasma treatment.

Device characterization: All of the electrical characterizations were done with the use of PBS as the electrolyte. The electrical properties of the OECT-based sensors were obtained by using a Keithley 2602 source meter with customized LabVIEW software. A CHI660E electrochemical workstation (CH Instruments, Inc.) was used to characterize the electrochemical properties of the different gate electrodes in the PBS solution. The surface capacitances of the electrodes in the PBS solution were characterized by using potentiostat instruments (Autolab, PGSTAT302N) with a symmetric cell configuration. [33] The amplitude of the applied AC signal was 50 mV.

Supporting Information
Supporting Information is available from the Wiley Online Library or from the author.

Acknowledgements
The authors gratefully acknowledge the support from General Research Fund (GRF) under Grant No.HKU 710313E and 17200314, the National Natural Science Foundation of China (NSFC) and the Research Grants Council (RGC) of Hong Kong Joint Research Scheme under Grant No.N_HKU715/14, Innovation and Technology Support Programme under Grant No. ITS/186/13 HKU Seed funding programme for applied research 201511160032. (Supporting Information is available online from Wiley InterScience or from the author).

Received: ((will be filled in by the editorial staff))
Revised: ((will be filled in by the editorial staff))
Published online: ((will be filled in by the editorial staff))

[1] L. Kergoat, B. Piro, D. T. Simon, M. Pham, V. Noël, M. Berggren, *Adv. Mater.* **2014**, *26*, 5658.

[2] P. Lin, X. T. Luo I. Hsing, F. Yan, *Adv. Mater.* **2011**, *23*, 4035.

[3] M. Sessolo, J. Rivnay, E. Bandiello, G. G. Malliaras, H. J. Bolink, *Adv. Mater.* **2014**, *26*, 4803.

[4] D. Khodagholy, V. F. Curto, K. J. Fraser, M. Gurfinkel, R. Byrne, D. Diamond, G. G. Malliaras, F. Benito-Lopez, R. M. Owens, *J. Mater. Chem.* **2012**, *22*, 4440.

[5] G. Tarabella, A. G. Balducci, N. Coppedè, S. Marasso, P. D'Angelo, S. Barbieri, M. Cocuzza, P. Colombo, F. Sonvico, R. Mosca, S. Iannotta, *Biochim. Biophys. Acta* **2013**, *1830*, 4374.

[6] D. Khodagholy, T. Doublet, P. Quilichini, M. Gurfinkel, P. Leleux, A. Ghestem, Esma Ismailova, T. Herve, S. Sanaur, C. Bernard, G. G. Malliaras, *Nat. Commun.* **2013**, *4*, 1575.

[7] A. Williamson, M. Ferro, P. Leleux, E. Isdmailova, A. Kaszas, T. Doublet, P. Quilichini, J. Rivnay, B. Rózsa, G. Katona, C. Bernard, *Adv. Mater.* **2015**, *27*, 4405.

[8] J. Rivnay, P. Leleux, M. Ferro, M. Sessolo, A. Williamson, D. A. Koutsouras, D. Khodagholy, M. Ramuz, X. Strakosas, R. M. Owens, C. Benar, J.-M. Badier, C. Bernard, G. G. Malliaras, *Sci. Adv.* **2015**, *1*, 4.

[9] M. H. Bolin, K. Svennersten, D. Nilsson, A. Sawatdee, E. W. H. Jager, A. Richter-Dahlfors, M. Berggren, *Adv. Mater.* **2009**, *21*, 4379.

[10] L. H. Jimison, S. A. Tria, D. Khodagholy, M. Gurfinkel, E. Lanzarini, A. Hama, G. G. Malliaras, R. M. Owens, "Measurement of barrier tissue integrity with an organic electrochemical transistor." *Adv. Mater.* **2012**, *24*, 5919.

[11] C. L. Yao, Q. Q. Li, J. Guo, F. Yan, I. Hsing, *Adv. Healthcare Mater.* **2015**, *4*, 528.

[12] A. Campana, T. Cramer, D. T. Simon, M. Berggren, F. Biscarini, *Adv. Mater.* **2014**, *26*, 3874.

[13] P. Leleux, J. Rivnay, T. Lonjaret, J. Badier, C. Bénar, T. Hervé, P. Chauvel, G. G. Malliaras, *Adv. Healthcare Mater.* **2105**, *4*, 142.

[14] M. Yamaguchi, M. Mitsumori, Y. Kano, *IEEE Eng. Med. Biol. Mag.* **1998**, *17*, 59.

[15] Z. T. Zhu, J. T. Mabeck, C. C. Zhu, N. C. Cady, C. A. Batt, G. G. Malliaras, *Chem. Commun.* **2004**, *13*, 1556.

[16] D. J. Macaya, M. Nikolou, S. Takamatsu, J. T. Mabeck, R. M. Owens, G. G. Malliaras, *Sens. Actuators B* **2007**, *123*, 374.

[17] H. Tang, F. Yan, P. Lin, J. B. Xu, H. L. W. Chan, *Adv. Func. Mater.* **2011**, *21*, 2264.

[18] B. Phypers, T. Pierce, Contin. Educ. Anaesth. Crit. Care Pain 2006, 6, 128.

[19] M. Zhang, C. Liao, C. H. Mak, P. You, C. L. Mak, F. Yan, *Sci. Rep.* **2015**, *5*, 8311.

[20] D. Khodagholy, J. Rivnay, M. Sessolo, M. Gurfinkel, P. Leleux, L. H. Jimison, E. Stavrinidou, T. Herve, S. Sanaur, R. M. Owens, G. G. Malliaras, *Nat. Commun.* **2013**, *4*, 2133.

[21] O. Yaghmazadeh, F. Cicoira, D. A. Bernards, S. Y. Yang, Y. Bonnassieux, G. G. Malliaras, *J. Polym. Sci. Part B: Polym. Phys.* **2011**, *49*, 34.

[22] F. Cicoira, M. Sessolo, O. Yaghmazadeh, J. A. DeFranco, S. Y. Yang, G. G. Malliaras, *Adv. Mater.* **2010**, *22*, 1012.

[23] D. A. Bernards, D. J. Macaya, M. Nikolou, J. A. DeFranco, S. Takamatsu, G. G. Malliaras, *J. Mater. Chem.* **2008**, *18*, 116.

[24] J. L. Lan, Y. Y. Wang, C. C. Wan, T. C. Wei, H. P. Feng, C. Peng, H. P. Cheng, Y. H. Chang, W. C. Hsu, *Curr. Appl. Phys.* **2010**, *10*, S168.

[25] C. Aliaga, J. Y. Park, Y. Yamada, H. S. Lee, C. K. Tsung, P. Yang, G. A. Somorjai, *J. Phys. Chem. C* **2009**, *113*, 6150.

[26] Y. Borodko, S. M. Humphrey, T. D. Tilley, H. Frei, G. A. Somorjai, *J. Phys. Chem. C* **2007**, *111*, 6288.

[27] J. M. Green, R. C. Pritchett, T. R. Crews, J. R. McLester, Jr., D. C. Tucker, *Eur. J. Appl. Physiol.* **2004**, *91*, 1.

[28] W. B. Nowall, W. G. Kuhr, *Anal. Chem.* **1995**, *67*, 3583.

[29] C. Z. Liao, C. H. Mak, M. Zhang, H. L. W. Chan, F.Yan, *Adv. Mater.* **2015**, *27*, 676.

[30] C. Jurysta, N. Bulur, B. Oguzhan, I. Satman, T. M. Yilmaz, W. J. Malaisse, A. Sener, *J. Biomed. Biotechnol.* **2009**, 430426.

[31] T. C. Wei, C. C. Wan, Y. Y. Wang, *Appl. Phys. Lett.* **2006**, *88*, 103122.

[32] J. Rivnay, P. Leleux, M. Sessolo, D. Khodagholy, T. Hervé, M. Fiocchi, G. G. Malliaras, *Adv. Mater.* **2013**, *25*, 7010.

[33] T. C. Wei, C. C. Wan, Y. Y. Wang, C. M. Chen, H. S. Shiu, *J. Phys. Chem. C* **2007**, *111*, 4847.

Figure Captions

Figure 1. a) Schematic diagram of glucose sensor based on OECT integrated with microfluidic channel. b) Gate electrode modification of device. c) Transfer curve and corresponding transconductance curve of an OECT. V_{DS} is fixed at -0.2 V. d) Output curve of OECT.

Figure 2. a). Cyclic voltammograms of Au/Pt NPs electrode after UV-Ozone treatment (Line I) and Au/Pt NPs electrode after thermal annealing treatment (Line II) measured in PBS that contains 10 mM of $[Fe(CN)_6]^{3-/4-}$ redox probe. CV scan rate: 50 mV/s. b) Surface capacitances of Au/Pt NPs electrode after UV-Ozone treatment (Line I), Au/Pt NPs electrode after thermal annealing treatment (Line II) and bare Au electrode (Line III) characterized in PBS solution at different frequencies. The area of each electrode is 0.24 cm^2. c) AFM image of Au/Pt NPs electrode that underwent UV-Ozone post treatment, RMS roughness is 3.6 nm. d) AFM image of Au/Pt NPs electrode that underwent thermal annealing post treatment, RMS roughness is 5.1 nm.

Figure 3. a) Normalized current after injection of different concentrations of glucose in device that underwent UV-Ozone post treatment. b) Enlarged image of Fig 2a. c) Normalized current after injection of different concentrations of glucose in device that underwent thermal annealing post treatment. d) Comparison of effective gate voltage shifts between the two devices. For normalized current vs. time curves, V_{DS} is fixed at -0.2 V and V_G is fixed at 0.5 V.

Figure 4. a) Normalized current after injection of different concentrations of lactate, V_{DS} is fixed at -0.2 V and V_G is fixed at 0.5 V. b) Corresponding effective gate voltage shift induced by lactate with different concentrations.

Figure 5. a) Schematic diagram of multiple sensor. b) ~i). Normalized current after injection of analyte with different compositions. b) Pure PBS. c) 10^{-5} M lactate. d) 10^{-4} M lactate. e) 10^{-5} M glucose. f) 10^{-4} M glucose. g) 10^{-4} M lactate with 10^{-5} M glucose. h) 10^{-4} M glucose with 10^{-5} M lactate. i) 10^{-4} M glucose with 10^{-4} M lactate. V_{DS} is fixed at -0.2 V and V_G is fixed at 0.5 V.

Figure 6. a) Gate electrode modification for saliva glucose sensor with a thin layer of nafion. b) Calibration curve of effective gate voltage shift after injection of different concentrations of pure glucose solution. c) Effective gate voltage shift induced by different saliva samples. Calculated glucose concentration in saliva, P_1: 0.074 ± 0.003 mM ; P_2: 0.0485 ± 0.001 mM; P_3: 0.146 ± 0.014 mM and P_4: 0.22 ± 0.019 mM.

Figure 7. a) Schematic diagram of portable glucose sensor that can interact with smartphone. b) Left side is main interface of app. Right side is detection curve of glucose. X-axis represents the time scale (0.1 s of one count), Y-axis represents the real-time voltage measured. c) Circuit diagram within the data acquisition dock. d) Transfer curve of the OECT device after adding a resistor in drain source circuit. e) Comparison of glucose testing results between measurements based on source meter versus smartphone.

Graphical Abstract

Organic electrochemical transistor (OECT) based enzymatic biosensor exhibit great potential in detection metabolite concentration in body fluid and other biomedical applications. Modified OECT-based biosensors with poly(N-vinyl-2-pyrrolidone)-capped platinum nanoparticles and microfluidic channel shows not only high sensitivity on single analyte glucose or lactate but also compatible with multi-analyte sensing. The current device has excellent potential on real-time non-invasive healthcare diagnostic.

Supporting Information

Highly Sensitive Metabolite Biosensor based on Organic Electrochemical Transistor Integrated with Microfluidic Channel and Poly(N-vinyl-2-pyrrolidone)-Capped Platinum Nanoparticles

Xudong Ji, Ho Yuen Lau, Xiaochen Ren, Boyu Peng, Peng Zhai, Shien-Ping Feng and Paddy K. L. Chan[*]

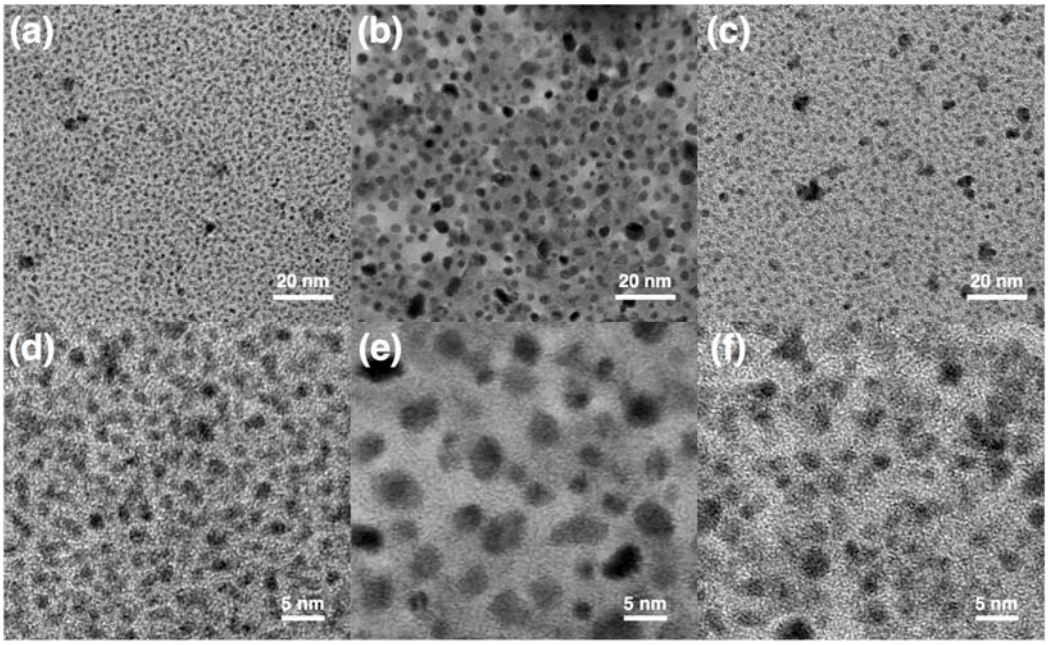

Figure S1. TEM images of PVP-capped platinum nanoparticles with different post treatment methods. a, d) Pristine sample. b, e) thermal annealing post treated sample. c, f) UV-Ozone post treated sample.

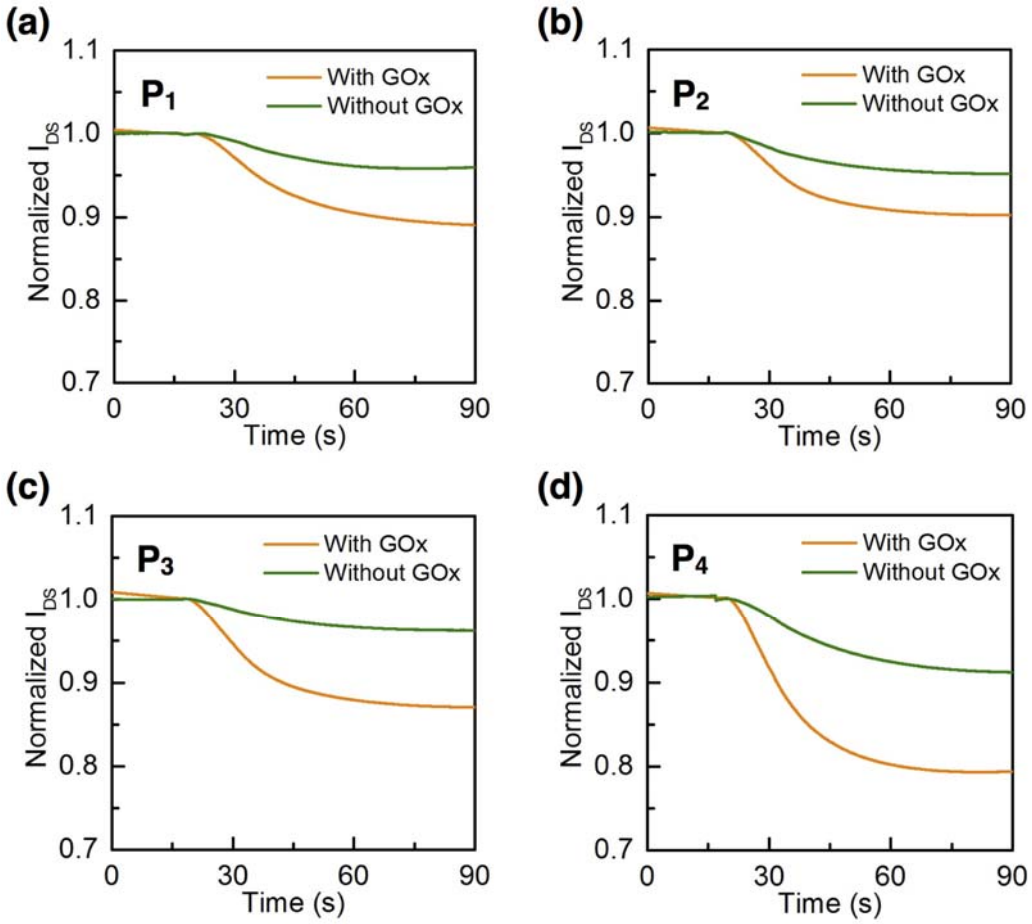

Figure S2. a, b) Normalized channel current induced by saliva from healthy individuals. c, d) Normalized channel current induced by saliva from diabetic patients. For normalized channel vs. time curves, V_{DS} is fixed at -0.2 V and V_G is fixed at 0.5V.

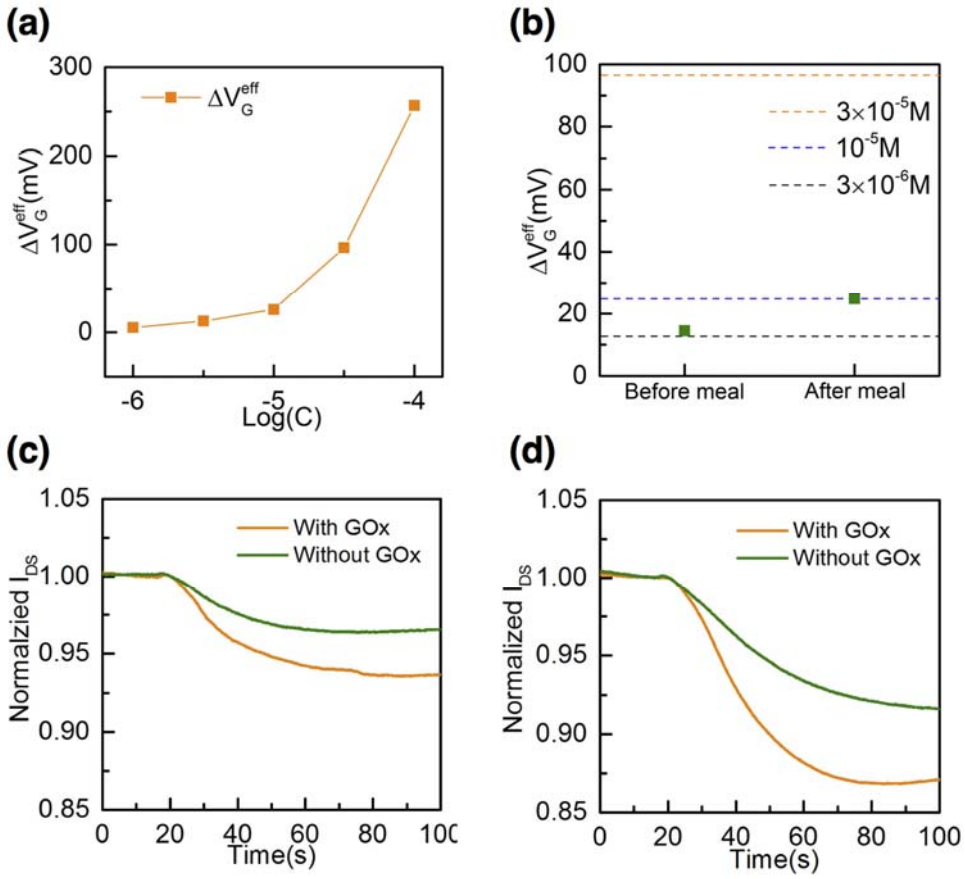

Figure S3. a) Calibration curve of effective gate voltage shift after injection of different concentrations of pure glucose solution. b) Effective gate voltage shift induced by saliva before and after meal. c) Normalized channel current induced by saliva before meal. d) Normalized channel current induced by saliva after meal. For normalized channel vs. time curves, V_{DS} is fixed at -0.2 V and V_G is fixed at 0.5 V.